tric materials in the canonical-wedge diffraction problem, which is not presently possible. Hence, for the present, the experimental approach is necessary.

Acknowledgment

The authors acknowledge the assistance of P. Gilon and Jeanne Shuler for programming and computational work, and helpful discussions with T. Charleton and R. F. Yang of the Andrew Corporation. Additionally, the help of O. C. Baldree, Jr., of NASA, who performed the bulk of the intricate antenna machine shop work, is gratefully acknowledged.

References

[1] P. W. Huber and T. Sims, "Research approaches to the problem of reentry communication," *Proc. AF Cambridge Research Center 3rd Plasma Sheath Symp.* (Bedford, Mass., September 21–23, 1965).

[2] C. R. Cockrell and W. F. Croswell, "The application of circular arrays to spacecraft antenna problems," *IEEE Trans. Aerospace*, vol. AS-2, pp. 272–277, April 1964.

[3] W. F. Croswell and C. M. Knop, "On the use of an array of circumferential slots on a large cylinder as an omnidirectional antenna," *IEEE Trans. Antennas and Propagation* (*Communication*), vol. AP-14, pp. 394–396, May 1966.

[4] J. B. Bangent *et al.*, "The Telstar experiment," *Bell Sys. Tech. J.*, vol. 42, pt. 1, pp. 869–897, July 1963.

[5] H. L. Knudsen, "Radiation from ring quasi-arrays," *IRE Trans. Antennas and Propagation*, vol. AP-4, pp. 452–472, July 1956.

[6] T. S. Chu, "On the use of uniform circular arrays to obtain omnidirectional patterns," *IRE Trans. Antennas and Propagation* (*Communications*), vol. AP-7, pp. 436–438, October 1959.

[7] J. R. Wait, *Electromagnetic Radiation From Cylindrical Structures*. New York: Pergamon, 1959, ch. 16.

[8] C. M. Knop, "The radiation fields from a circumferential slot on a metal cylinder coated with a lossy dielectric," *IRE Trans. Antennas and Propagation*, vol. AP-9, pp. 535–545, November 1961.

[9] C. R. Cockrell, "Computations for larger uniform circular arrays with typical elements patterns," NASA, Hampton, Va., Tech. Note NASA TN D-2105, October 1964.

[10] H. Gruenberg, "Theory of wave-guide-fed slots radiating into parallel-plate regions," *J. Appl. Phys.*, vol. 23, pp. 733–737, July 1952.

[11] A. F. Stevenson, "Theory of slots in rectangular waveguides," *J. Appl. Phys.*, vol. 19, pp. 733–737, 1948.

[12] J. F. Ramsay and B. V. Popovich, "Series-slotted waveguide array antennas," *1963 IEEE Internat'l Conv. Rec.*, pt. 1, pp. 30–55.

[13] W. F. Croswell and R. B. Higgins, "Effects of dielectric covers over shunt slots in a waveguide," NASA, Hampton, Va., Tech. Note NASA TN D-2518, December 1964.

[14] R. S. Elliot, "Azimuthal surface waves on circular cylinders," *J. Appl. Phys.*, vol. 26, pp. 368–376, April 1955.

[15] M. C. Bailey, "Design of dielectric covered resonant slots in a rectangular waveguide," *IEEE Trans. Antennas and Propagation*, vol. AP-15, pp. 594–598, September 1967.

[16] C. H. Walter, *Traveling Wave Antennas*. New York: McGraw-Hill, 1965, pp. 225–233.

Application of Spherical Wave Theory to Cassegrainian-Fed Paraboloids

PHILIP D. POTTER, MEMBER, IEEE

Abstract—**In this paper the spherical wave expansion technique is used to analyze the general properties of paraboloidal antenna feed systems. As a result, fundamental aperture efficiency and noise temperature limitations are established as quantitative functions of antenna wavelength size. A boundary-value solution is found for synthesis of ideal subreflector shapes in a Cassegrain-type feed system. The resulting surface is found to reduce the classical hyperboloid in the limit of zero wavelength. Applications of this synthesis technique to high performance feed systems and subreflector matching are discussed. Finally, an interesting quantitative cross-check between vector spherical wave and vector diffraction theories is obtained.**

I. Introduction

THE two-reflector antenna system invented for optical frequency use by Cassegrain has achieved widespread interest and usage in the microwave antenna field. Because Cassegrainian systems are typically used in electrically large antenna installations, geometric optics techniques have been generally used for design and analysis.[1]–[4] Some performance parameters are not quantitatively predictable from geometric optics, however, and as a result a number of diffraction analyses have been published.[5]–[8]

Although the optically-derived subreflector is the simplest and most practical for many applications, other surfaces may offer performance advantages in terms of aperture efficiency and spillover.[9]–[15] This paper considers a synthesis technique which proceeds along different lines from those previously presented. The feed system is defined such as to produce a spherical wavefront at infinity within a specified angular region. The amplitude radiation pattern is defined as a best-fit to a specified "ideal" pattern, within the constraints of finite feed system and main reflector sizes. A spherical wave expansion technique is then used to derive a subreflector contour and feed horn radiation pattern which yields the required feed system radiation patterns. The question of physically realizing the resulting required feed horn radiation patterns has been discussed in detail by Ludwig[16] and is not analyzed here.

Manuscript received December 30, 1966; revised May 31, 1967. This paper presents the results of one phase of research carried out at the Jet Propulsion Laboratory, California Institute of Technology, under Contract NAS 7-100, sponsored by NASA.

The author is with the Jet Propulsion Laboratory, Pasadena, Calif.

II. Spherical Waves

As a useful idealization, the region between the main paraboloidal reflector and the feed system may be considered to be a source-free, homogeneous, isotropic medium with zero conductivity. Under these conditions, the electric and magnetic fields are completely described by the homogeneous vector wave equations

$$\nabla(\nabla\cdot\boldsymbol{E}) - \nabla\times(\nabla\times\boldsymbol{E}) + k^2\boldsymbol{E} = 0 \tag{1}$$

$$\nabla(\nabla\cdot\boldsymbol{H}) - \nabla\times(\nabla\times\boldsymbol{H}) + k^2\boldsymbol{H} = 0 \tag{2}$$

where

$\boldsymbol{E}$ = electric field
$\boldsymbol{H}$ = magnetic field
k = free space propagation constant.

The solutions to (1) and (2) in spherical coordinates are discussed in detail by Stratton.[17] Three families of independent vector solutions exist, designated $\boldsymbol{M}_{mn}$, $\boldsymbol{N}_{mn}$, and $\boldsymbol{L}_{mn}$. The last of these represents a family of plane waves and need not be considered further. The $\boldsymbol{M}_{mn}$ and $\boldsymbol{N}_{mn}$, however, describe the complex $\boldsymbol{E}$ and $\boldsymbol{H}$ fields of families of transverse electric (TE) and transverse magnetic (TM) waves. The field components are as follows:

TE_{mn} waves

$$\boldsymbol{E}_{mn} = jZ_0\boldsymbol{M}_{mn} \tag{3}$$

$$\boldsymbol{H}_{mn} = \boldsymbol{N}_{mn} \tag{4}$$

TM_{mn} waves

$$\boldsymbol{E}_{mn} = \boldsymbol{N}_{mn} \tag{5}$$

$$\boldsymbol{H}_{mn} = \frac{j}{Z_0}\boldsymbol{M}_{mn} \tag{6}$$

where

$$Z_0 = \text{free space impedance.}$$

It can be shown[18] that in a source-free region between two concentric spheres (one of these may have infinite radius), only TE and TM waves can exist, therefore (3) to (6) constitute a complete solution to possible fields in the region between a feed system and the main reflector. This set of waves is directly analogous to the set of modes which may exist in a waveguide; a complete knowledge of mode strengths at one point in space uniquely determines the fields (in amplitude, phase, and direction) elsewhere.

In describing the feed system fields, a right-handed polar coordinate system is used, as shown in Fig. 1. The vector functions $\boldsymbol{M}_{mn}$ and $\boldsymbol{N}_{mn}$ are given in terms of the polar angle ψ, the azimuthal angle ξ, the radius ρ, and the associated unit vectors. The assumed time dependence $e^{j\omega t}$ will be suppressed throughout this paper. Expressions for $\boldsymbol{M}_{mn}$ and $\boldsymbol{N}_{mn}$ are as follows:

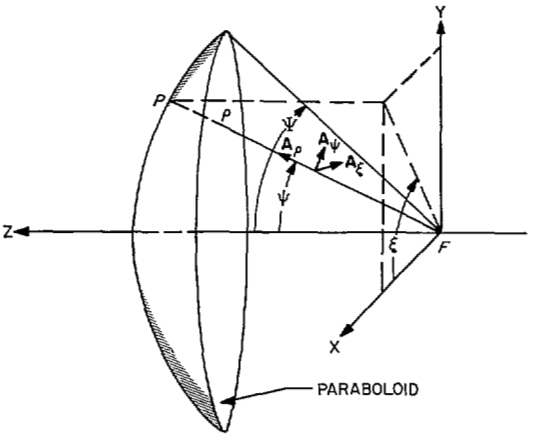

Fig. 1. Paraboloid geometry.

$$\boldsymbol{M}_{mn} = \mp\frac{m}{\sin\psi}Z_n(k\rho)P_n^m(\cos\psi)\begin{bmatrix}\sin\\ \cos\end{bmatrix}m\xi\boldsymbol{a}_\psi - Z_n(k\rho)\frac{d}{d\psi}[P_n^m(\cos\psi)]\begin{bmatrix}\cos\\ \sin\end{bmatrix}m\xi\boldsymbol{a}_\xi \tag{7}$$

$$\boldsymbol{N}_{mn} = \frac{1}{k\rho}\frac{d}{d\rho}[\rho Z_n(k\rho)]\frac{d}{d\psi}[P_n^m(\cos\psi)]\begin{bmatrix}\cos\\ \sin\end{bmatrix}m\xi\boldsymbol{a}_\psi \mp\frac{m}{k\rho\sin\psi}\frac{d}{d\rho}[\rho Z_n(k\rho)]P_n^m(\cos\psi)\begin{bmatrix}\sin\\ \cos\end{bmatrix}m\xi\boldsymbol{a}_\xi + \frac{n(n+1)}{k\rho}Z_n(k\rho)P_n^m(\cos\psi)\begin{bmatrix}\cos\\ \sin\end{bmatrix}m\xi\boldsymbol{a}_\rho \tag{8}$$

where $P_n^m(\cos\psi)$ is the associated Legendre polynomial of the first kind[19] and $Z_n(k\rho)$ is the spherical Bessel function.[17] For the problem under consideration, the spherical waves must satisfy the radiation condition at infinity and hence the spherical Bessel functions are restricted to be spherical Hankel functions $h_n^{(2)}(k\rho)$. Tables of all of the involved functions are available.[20]–[22]

A. Restriction of Wave Order

The spherical waves given by (3) to (8) possess the orthogonality properties familiar in guided waves; a member of a set of these waves, excited by the feed system, maintains independence throughout free space with a constant total propagation power. Although each wave is a separable function of ψ, ξ, and ρ, this is not generally true of a sum of these waves; the sum may change character completely as a function of ρ. Of interest is the asymptotic behavior of the radial functions $h_n^{(2)}(k\rho)$:

Far-field region, $k\rho \gtrsim n^2$

$$h_n^{(2)}(k\rho) \approx (j)^{(n+1)}\frac{e^{-jk\rho}}{k\rho} \tag{9}$$

$$\frac{1}{k\rho}\frac{d}{d\rho}[\rho h_n^{(2)}(k\rho)] \approx (j)^n\frac{e^{-jk\rho}}{k\rho} \tag{10}$$

Fresnel region, $n \lesssim k\rho \gtrsim n^2$

$$h_n^{(2)}(k\rho) \approx (j)^{(n+1)} \frac{e^{-jkf_1(\rho,n)}}{k\rho} \tag{11}$$

$$\frac{1}{k\rho}\frac{d}{d\rho}\left[\rho h_n^{(2)}(k\rho)\right] \approx (j)^n \frac{e^{-jkf_2(\rho,n)}}{k\rho} \tag{12}$$

Near-field region, $0 \gtrsim k\rho \lesssim n$

$$h_n^{(2)}(k\rho) = f_3(\rho, n) \tag{13}$$

$$\frac{1}{k\rho}\frac{d}{d\rho}\left[\rho h_n^{(2)}(k\rho)\right] = f_4(\rho, n) \tag{14}$$

where $f_1(\rho, n)$, $f_2(\rho, n)$, $f_3(\rho, n)$, and $f_4(\rho, n)$ indicate complicated dependence upon ρ and n.

In the far-field region, all of the spherical waves suffer inverse-distance amplitude decay and all remain essentially in phase synchronism. In the Fresnel region, the waves have essentially this same amplitude dependence, but they do not maintain phase synchronism as a function of $k\rho$. In the near field, the waves behave nonsimply in both amplitude and phase.

Numerical investigation of the Hankel functions shows that the quantities $f_3(\rho, n)$ and $f_4(\rho, n)$ in (13) and (14) assume very large values for $k\rho \ll n$. This fact implies a possible supergain situation which has been investigated by several authors.[23]–[25] For large-wavelength two-reflector antenna systems, a different restriction upon N is more significant. This latter restriction, qualitatively indicated by (11) and (12), arises from a requirement that the paraboloidal main reflector be in the far-field region of the subreflector scattered fields to within some specified phase error tolerance. In Appendix I it is shown that the far-field restriction may be quantitatively expressed as follows:

$$N \leq B\sqrt{kf} = B\left[2\pi\left(\frac{f}{D}\right)\left(\frac{D}{\lambda}\right)\right]^{1/2} \tag{15}$$

where

B = a constant
f = paraboloid focal length
D = paraboloid diameter
λ = wavelength of operation.

Choice of the constant B will be a function of the wave amplitudes versus n and of the desired phase error at the paraboloid. Numerical investigation shows that the phase error effect is typically small for $B=1$ and severe for $B=2$.

The azimuthal index m is restricted to one since only these waves will radiate axially from the paraboloid.[8] Thus the general feed system radiation path may be expressed as a sum of TE_{1n} and TM_{1n} waves, where $1 \leq n \leq N$. Waves of the form TE_{10} and TM_{10} are not possible because of the properties of the associated Legendre polynomials which require that

$$n \geq m. \tag{16}$$

B. Feed System Expansion in Spherical Waves

The general expression for the feed system radiation pattern $E_f(\psi, \xi, \rho)$ is given as follows:

$$E_f(\psi, \xi, \rho) = \sum_{n=1}^{n=N} \left[A_{TE_{1n}} \boldsymbol{E}_{TE_{1n}} + A_{TM_{1n}} \boldsymbol{E}_{TM_{1n}}\right] \tag{17}$$

where

$A_{TE_{1n}}$, $A_{TM_{1n}}$ = complex wave coefficients.

$\boldsymbol{E}_{TE_{1n}}$ and $\boldsymbol{E}_{TM_{1n}}$ are given by (3) to (8) with obvious notation changes.

In the far field, the asymptotic expressions (9) and (10) may be used to simplify, yielding

$$\boldsymbol{E}_{TE_{1n}} = \frac{-(j)^n Z_0 e^{-jk\rho}}{k\rho}\left[\frac{P_n^1(\cos\psi)}{\sin\psi}\sin\xi \boldsymbol{a}_\psi + \frac{dP_n^1(\cos\psi)}{d\psi}\cos\xi \boldsymbol{a}_\xi\right] \tag{18}$$

$$\boldsymbol{E}_{TM_{1n}} = \frac{+(j)^n e^{-jk\rho}}{k\rho}\left[\frac{dP_n^1(\cos\psi)}{d\psi}\sin\xi \boldsymbol{a}_\psi + \frac{P_n^1(\cos\psi)}{\sin\psi}\cos\xi \boldsymbol{a}_\xi\right]. \tag{19}$$

A class of idealized, azimuthally-symmetric feed system patterns is chosen which eliminates aperture cross polarization[8] and also eliminates the feed system backlobe (see Appendix B).

$$\boldsymbol{E}_f(\psi, \xi, \rho) \triangleq \frac{e^{-jk\rho}}{k\rho}(\sin\xi \boldsymbol{a}_\psi + \cos\xi \boldsymbol{a}_\xi)F(\psi) \tag{20}$$

where $F(\psi)$ is the desired polar pattern.

Standard techniques are applied to (17) to (20) (see Stratton[17]) to obtain the wave coefficients

$$A_{TE_{1n}} = \frac{-(-j)^n(2n+1)}{2Z_0 n^2(n+1)^2}\int_0^\pi F(\psi)\cdot\left[\frac{P_n^1(\cos\psi)}{\sin\psi} + \frac{dP_n^1(\cos\psi)}{d\psi}\right]\sin\psi d\psi \tag{21}$$

$$A_{TM_{1n}} = -Z_0 A_{TE_{1n}}. \tag{22}$$

For numerical use, it is convenient to define certain normalized functions as follows:

$$f_n(\psi) \triangleq \frac{1}{n(n+1)}\left[\frac{P_n^1(\cos\psi)}{\sin\psi} + \frac{dP_n^1(\psi)}{d\psi}\right] \tag{23}$$

$$A_n \triangleq \frac{Z_0 n(n+1)}{-(-j)^n} A_{TE_{1n}} = \frac{2n+1}{2}\int_0^\pi F(\psi) f_n(\psi)\sin\psi d\psi. \tag{24}$$

From (17) through (24), the feed system far-field radiation

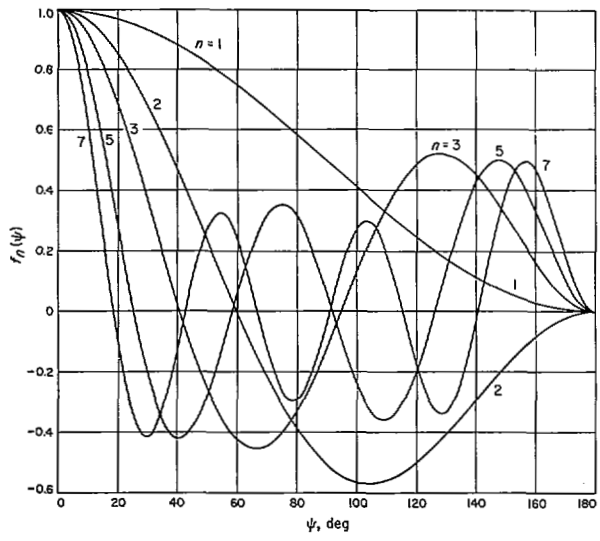

Fig. 2. Elemental wave functions $fn(\psi)$.

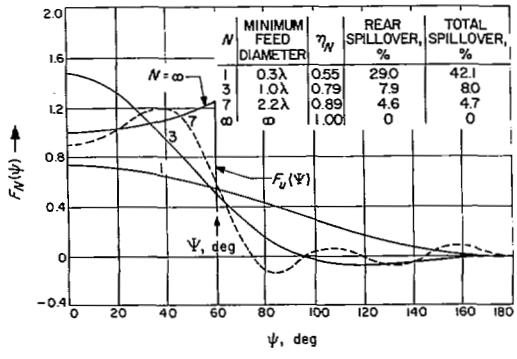

Fig. 3. Synthesis of ideal illumination pattern.

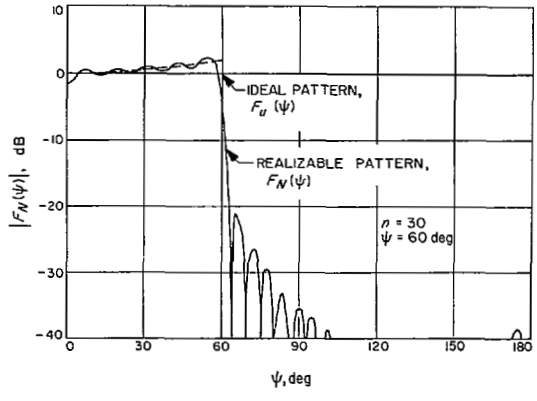

Fig. 4. Spherical wave fit to ideal illumination pattern.

patterns are given as

$$E_{f_N}(\psi, \xi, \rho) = \frac{e^{-jk\rho}}{k\rho}(\sin \xi a_\psi + \cos \xi a_\xi) F_N(\psi) \quad (25)$$

$$F_N(\psi) = \sum_{n=1}^{n=N} A_n f_n(\psi) \quad (26)$$

where $F_N(\psi)$ is the spherical wave fit to the desired generalized polar pattern $F(\psi)$. A plot of the first few of the elemental wave functions, $f_n(\psi)$, is shown in Fig. 2.

C. Uniform Illumination Case

As a special case of considerable practical importance, $F(\psi)$ may be chosen such as to provide uniform aperture illumination over a specified angular region and no radiation elsewhere.

$$F_u(\psi) \triangleq \sec^2\left(\frac{\psi}{2}\right), \quad \psi_1 \le \psi \le \psi_0$$

$$F_u(\psi) \triangleq 0, \qquad 0 \le \psi < \psi_1 \text{ and } \psi_0 < \psi \le \pi. \quad (27)$$

For this case, the integration in (24) may be performed in closed form, resulting in a simple expression for A_n:

$$A_n(\psi_0, \psi_1) = \frac{2n+1}{n(n+1)}\left[\tan\left(\frac{\psi_0}{2}\right) P_n^1(\cos\psi_0) - \tan\left(\frac{\psi_1}{2}\right) P_n^1(\cos\psi_1)\right]. \quad (28)$$

If ψ_1 is selected to be zero, then the predicted aperture efficiency asymptotically approaches unity as N becomes large; similarly, the total spillover approaches zero as N becomes large.

Fig. 3 shows the spherical wave fits to (27) which are obtained for small N; Fig. 4 shows the excellent fit which is achieved for $N=30$. In the following section, the variation of performance with N and antenna size is quantitatively investigated.

III. Fundamental Performance Limitations

This section parallels in part independent work by personnel of the Hughes Aircraft Company;[27] the results are included here because of their relationship to the synthesis procedure described in the following section.

A. Aperture Efficiency

The system aperture efficiency η is given by[4]

$$\eta = \frac{2\cot^2\left(\frac{\psi}{2}\right)\left|\int_0^{\psi} F_N(\psi)\tan\left(\frac{\psi}{2}\right)d\psi\right|^2}{\int_0^{\pi} |F_N(\psi)|^2 \sin\psi d\psi} \quad (29)$$

where

ψ = edge angle of the paraboloid.

With use of (23) through (29), a general closed-form expression may be obtained for aperture efficiency

$$\eta = \frac{\left|\sum_{n=1}^{N} \frac{A_n}{n(n+1)} P_n^1(\cos\psi)\right|^2}{\sum_{n=1}^{N} \frac{A_n^2}{2n+1}}. \quad (30)$$

In general, numerical integration will be necessary to determine the wave coefficients A_n. For the important special case of a fit to uniform illumination (see Section II-C)

$$\eta = \frac{\left| \sum_{n=1}^{N} \frac{2n+1}{n^2(n+1)^2} P_n^1(\cos\psi) P_n^1(\cos\psi_0) \right|^2}{\sum_{n=1}^{N} \frac{2n+1}{n^2(n+1)^2} [P_n^1(\cos\psi_0)]^2} \tag{31}$$

where

ψ_0 = the pattern cutoff angle in the ideal pattern $F(\psi)$.

It is readily shown that a choice of $\psi = \psi_0$ will maximize η; this choice results in a compact form for (31)

$$\eta_{\max} = \sum_{n=1}^{N} \frac{2n+1}{n^2(n+1)^2} [P_n^1(\cos\psi)]^2 = 2 \sum_{n=1}^{N} \frac{[\overline{P}_n^1(\cos\psi)]^2}{n(n+1)} \tag{32}$$

where

$\overline{P}_n^1(\cos\psi)$ = *normalized* associated Legendre polynomial.[21] In order to establish fundamental aperture efficiency limitations, it is necessary to relate N to antenna wavelength size by use of (15), which may be expressed

$$N = B\left[\frac{\pi}{2} \operatorname{ctn}\left(\frac{\psi}{2}\right)\left(\frac{D}{\lambda}\right)\right]^{1/2}. \tag{33}$$

Fig. 5 is a plot of (32) for selected values of aperture half angle ψ; smooth curves have been established between the integral values of n because these integral values do not appear to have special physical significance. As indicated by Fig. 2, a minimum n is required to efficiently synthesize a pattern for a given ψ. As shown in Fig. 5, the aperture efficiency rises rapidly for N values smaller than this critical value.

Fig. 6 is a plot of (33) for the case of $B=1$ and various aperture half angles. Combining these curves with those of Fig. 5, a plot of aperture efficiency versus aperture angular size may be constructed as shown in Fig. 7. The conflicting ψ dependences in the two previous figures largely compensate, with a result that fundamental aperture efficiency limitations are largely independent of f/D value. The degree to which these high performance levels are achievable in practice depends primarily on the state-of-the-art in feed horn design[16] and upon other practical considerations such as subreflector support design.[11] At present, overall efficiency is constrained by these considerations to about 70 percent. The subreflector blockage effect may be made negligibly small, since the spherical wave constraint is far-field distance rather than subreflector size (see Section II-A).

B. Figure of Merit

If the antenna system is to be used in a low-noise receiving configuration, it is appropriate to define an antenna figure-of-merit (FM), which is the quotient of aperture efficiency and system noise temperature

$$FM \triangleq \frac{\eta T_0}{T_0 + T_s} \tag{34}$$

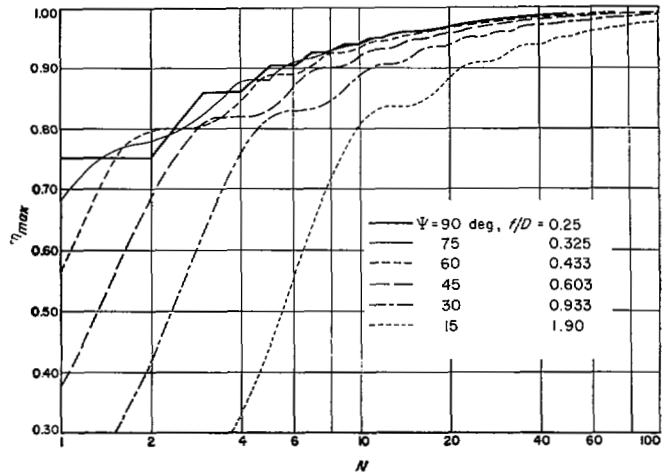

Fig. 5. Maximum aperture efficiency as a function of wave order.

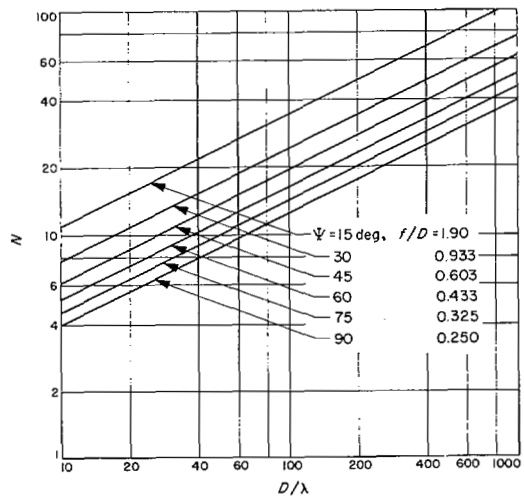

Fig. 6. Wave order as a function of aperture size.

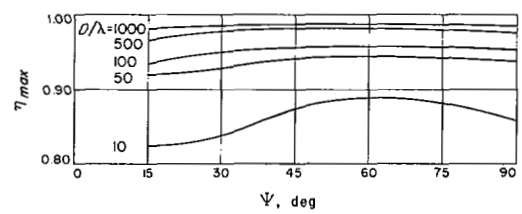

Fig. 7. Maximum aperture efficiency versus aperture angular size.

where

$T_s \triangleq 240°$ Kelvin $\times$ (fractional rear hemisphere spillover) (35)

$T_0 \triangleq$ (total system noise temperature) $- T_s$. (36)

Equation (35) is not rigorous; however, it is mathematically convenient and sufficiently accurate for FM optimization. For this optimization, the paraboloid edge angle ψ is varied in the region of the pattern cutoff angle ψ_0 such as to maximize (34). A parameter $\Delta\psi_{opt}$ may be defined such that (34) is optimized

$$\Delta\psi_{opt} \triangleq \psi_{opt} - \psi_0. \tag{37}$$

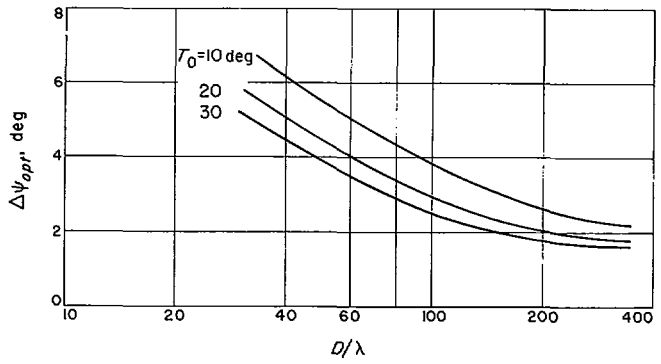

Fig. 8. $\Delta\psi_{opt}$ as a function of aperture size.

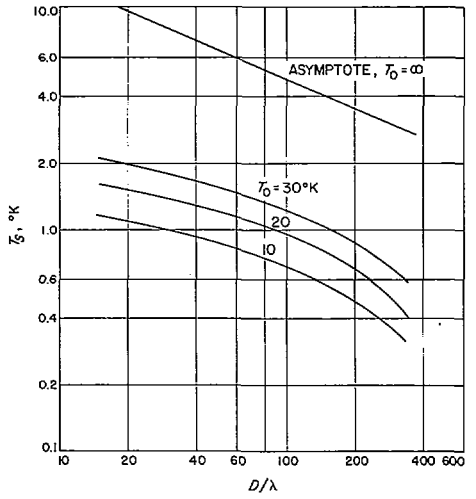

Fig. 9. Optimized spillover noise versus aperture size.

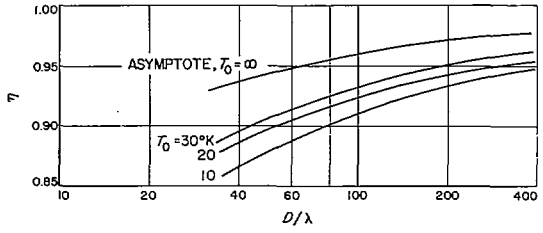

Fig. 10. Optimized aperture efficiency versus aperture size.

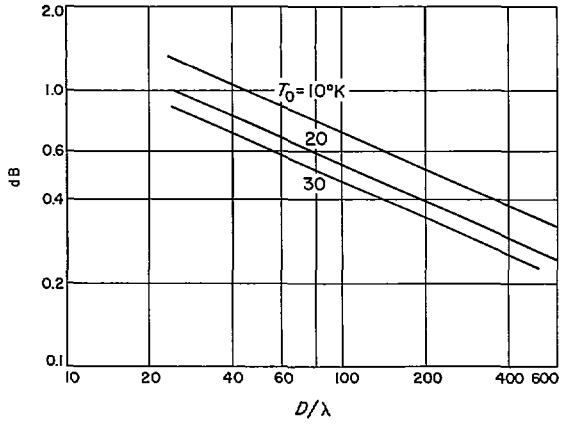

Fig. 11. Figure-of-merit versus aperture size.

Fig. 8 shows this parameter for the case of $\psi_0=60°$. It should be noted that $\Delta\psi_{opt}$ will always be positive and approaches zero for large N and high system noise temperature. Figs. 9 and 10 show, respectively, the corresponding spillover noise contribution and aperture efficiency achieved by use of $\Delta\psi_{opt}$. Finally, Fig. 11 shows FM as a function of aperture size. The following section considers a synthesis technique for realizing the performance levels shown in Figs. 9 to 11.

IV. Spherical Wave Synthesis of Nonoptical Subreflectors

Fig. 12 shows the assumed geometry of the Cassegrain-type paraboloidal antenna feed system. In this section, a general equation for the desired surface is obtained; for the limiting case of a spherical wave from the feed horn and vanishing wavelength, the surface equation reduces to that of a hyperboloid.

The total vector field E_T in the vicinity of the subreflector is the sum of the incident field E_H from the feed horn and the scattered field E_s.

$$E_T = E_H + E_s. \tag{38}$$

A general horn pattern E_H is assumed as follows:

$$E_H \triangleq -\frac{[F_{H\gamma}(\gamma)\sin\xi a_\gamma + F_{H\xi}(\gamma)\cos\xi a_\xi]}{kr} \cdot e^{-jk}\left[r - 2a - \frac{\delta_H(\gamma)}{k}\right] \tag{39}$$

where

$F_{H\gamma}(\gamma)$ = feed horn polar radiation pattern
$F_{H\xi}(\gamma)$ = feed horn azimuthal radiation pattern
a = a geometrical constant
$\delta_H(\gamma)$ = feed horn phase pattern, assumed to be azimuthally symmetric.

The scattered field E_s is now set equal to the sum of spherical wave functions

$$E_s \triangleq F(\psi, \rho)(\sin\xi a_\psi + \cos\xi a_\xi) \tag{40}$$

where

$$F(\psi, \rho) = jZ_0 \sum_{n=1}^{n=N} a_{TE_n} h_n(k\rho)\left[\frac{P_n^1(\psi)}{\sin\psi} + \frac{dP_n^1(\psi)}{d\psi}\right]. \tag{41}$$

Equation (41) may be expressed as having a quasi-spherical wavefront, as follows:

$$F(\psi, \rho) \triangleq \frac{F_s(,\psi\ \rho)}{\rho} e^{-j[k\rho - \delta(\rho,\psi)]}. \tag{42}$$

The restriction is now imposed that the subreflector be a surface of revolution. This restriction considerably simplifies the problem and results in a polarization independent solu-

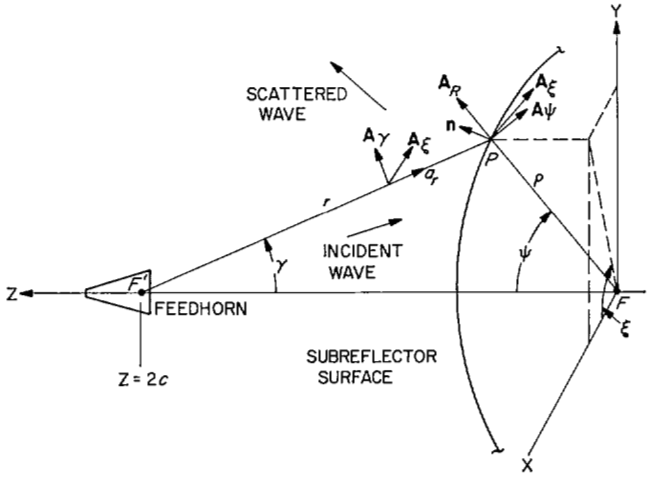

Fig. 12. Feed system geometry.

tion. From (38) to (42), two equations result:

$$F_{H\xi}(\gamma) = \frac{r}{\rho} F_s(\psi, \rho) = \frac{\sin \psi}{\sin \gamma} F_s(\psi, \rho) \tag{43}$$

$$\rho = \frac{c^2 - \left[a - \dfrac{\lambda\delta(\rho, \psi) - \lambda\delta_H(\gamma)}{4\pi}\right]^2}{c \cos \psi + a - \dfrac{\lambda\delta(\rho, \psi) - \lambda\delta_H(\gamma)}{4\pi}}, \tag{44}$$

and from the electric field boundary condition

$$\frac{F_{H\xi}(\gamma)}{F_{H\gamma}(\gamma)} = \cos(\psi + \gamma) - \frac{1}{\rho} \sin(\psi + \gamma) \frac{d\rho}{d\psi} \tag{45}$$

where $d\rho/d\psi$ is evaluated on the surface. Of interest is

$$\lim_{\lambda \to 0} \rho = \frac{c^2 - a^2}{c \cos \psi + a}, \tag{46}$$

which is the polar equation of the classical optically derived hyperboloid.

A. Comparison with Scattering Theory

Equation (44) defines an infinite subreflector surface which, when used with the feed horn patterns given by (43) and (45), will result in the high performance levels predicted in Section III. A computer program[28] has been written for the IBM 7094 to generate the required surface and feed horn patterns, given a few simple inputs such as N, λ, a, and c.

In any physical system, the subreflector must be truncated; it is intuitively suspected that truncation will be a small effect, as long as the truncation occurs in the region of low feed horn illumination. The effect of truncation has been quantitatively investigated by means of the subreflector scattering program.[8],[28] The latter uses the current integration method to numerically evaluate the scattered fields from a subreflector of revolution with arbitrary contour and illumination.

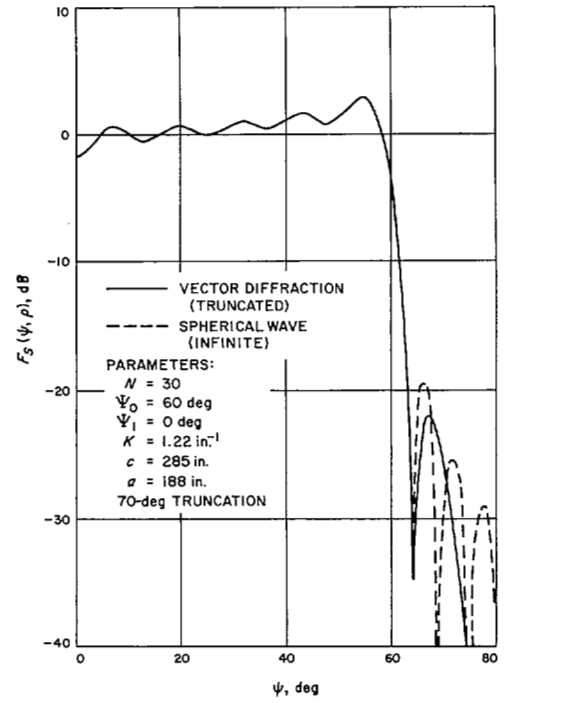

Fig. 13. Comparison of scattered fields by spherical wave and vector diffraction methods.

Fig. 13 shows a comparison of the scattered fields for the spherical wave formulation with those predicted by the current integration technique. The excellent agreement shown in Fig. 13 serves not only as a check on the spherical wave formulation but also as an unusual cross check between two completely different branches of electromagnetic theory. Of more practical significance is the demonstration that the ideal infinite subreflector may be truncated to a physically reasonable configuration without significant performance degradation. From Fig. 13 it can be seen that rear hemisphere spillover is essentially unchanged by a reasonable truncation. Also, it has already been shown[11] that the effect of forward spillover can be made negligibly small with a truncated subreflector.

B. Characteristics of the Synthesized Feed System

A typical required feed horn pattern is shown in Fig. 14, together with a four-waveguide-mode conical horn pattern as proposed by Ludwig.[16] As pointed out by Ludwig,[16] this four-mode pattern corresponds to $N \approx 25$ for a spherical wave synthesis of the horn pattern.

The nature of the synthesized subreflector surface is shown in Fig. 15 for the same case depicted in Fig. 14. Also shown is the experimentally derived nonoptical subreflector described in Potter.[10] The latter is seen to be an excellent fit to the spherical wave synthesis result. The case of $\alpha = 18.5°$ corresponds exactly to the shaped subreflector used in Potter.[11] The general result of a positive deviation beyond the optical edge at $\Psi = \psi$ appears to follow naturally from the requirement to use the feed horn pattern edge energy effectively; a similar result has been obtained with optical synthesis techniques.[14]

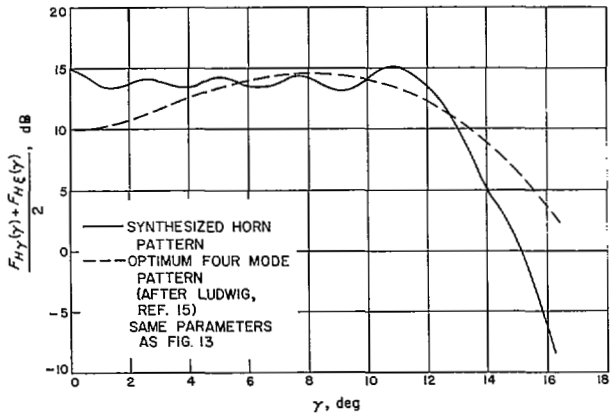

Fig. 14. Synthesized horn radiation patterns.

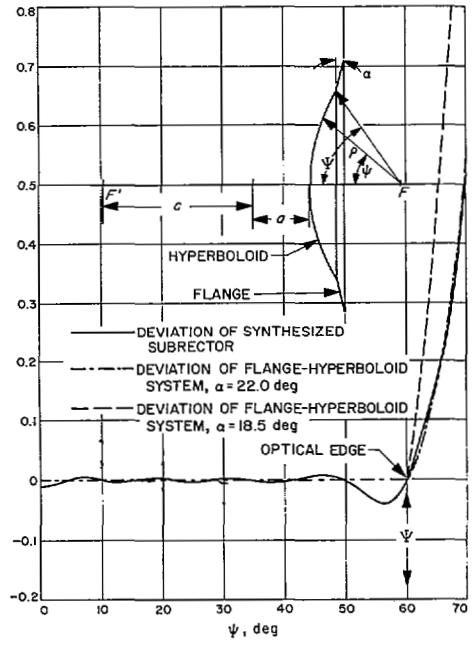

Fig. 15. Subreflector deviation from the optical case.

C. Application to Subreflector Matching

One of the most interesting applications of the spherical wave synthesis technique is that of subreflector matching. It is a simple matter to design such matching devices for prevention of subreflector scattering in the feed horn direction. A more difficult matter, however, is to design the vertex plate such that the redirected energy is used constructively in the antenna system. This latter problem is not amenable to solution by optical techniques because of the small wavelength sizes and radii of curvature involved. The boundary-value nature of the spherical wave technique is thus ideally suited to the problem.

Since the normalized wave functions $f_n(\Psi)$ are all unity for $\psi=0$ (see Fig. 2), the scattered axial far field is given simply by the sum of the coefficients A_n [see (26)]. Fig. 16 shows a comparison of a synthesized spherical wave vertex

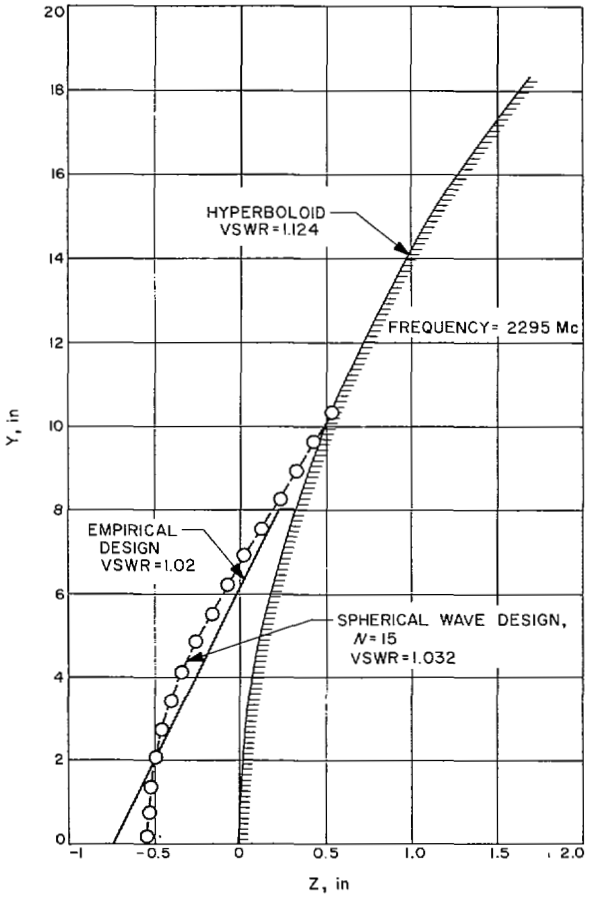

Fig. 16. Vertex plate designs.

plate with one which was previously empirically designed for good match and minimal effect upon the aperture efficiency. The VSWR values for the unmatched hyperboloid and the synthesized surface were calculated using standard current-integration techniques[29] and assuming a conventional horn pattern rather than the synthesized pattern.

V. Conclusions

Spherical wave theory has been applied in detail to the Cassegrainian-fed paraboloid design. Several applications of the method have been noted, including improved aperture illumination, reduced spillover and improved subreflector impedance matching. Perhaps the most important contribution of this analysis is to provide physical understanding to an important diffraction problem which is beyond the capabilities of geometric optics and which may be only crudely treated by geometric diffraction methods.

Appendix A
Spherical Wave Phase Error

A useful asymptotic expansion for the spherical Hankel functions has been developed by Stratton[17]

$$h_n^{(2)}(k\rho) = \frac{j^{(n+1)}}{k\rho} e^{-jk\rho}\left[P_{n+\frac{1}{2}}(k\rho) - jQ_{n+\frac{1}{2}}(k\rho)\right] \quad (47)$$

TABLE I

PHASE ERROR VERSUS τ

τ	$N=5$ (exact)	$N=5$ (approx.)	$N=10$ (exact)	$N=10$ (approx.)	$N=20$ (exact)	$N=20$ (approx.)	$N=50$ (exact)	$N=50$ (approx.)
0.250	−143.92°	−125.12°	−127.87°	−122.02°	−120.74°	−119.63°	−116.95°	−117.88°
0.500	−69.64	−74.71	−63.25	−69.74	−60.21	−66.74	−58.45	−64.79
1.000	−34.49	−35.80	−31.54	−32.86	−30.09	−31.31	−29.22	−30.38
2.000	−17.20	−17.39	−15.76	−15.94	−15.04	−15.20	−14.61	−14.76
4.000	−8.60	−8.62	−7.88	−7.90	−7.52	−7.54	−7.30	−7.32
8.000	−4.30	−4.30	−3.94	−3.94	−3.76	−3.76	−3.65	−3.65
16.000	−2.15	−2.15	−1.97	−1.97	−1.88	−1.88	−1.82	−1.82
32.000	−1.07	−1.07	−0.98	−0.98	−0.94	−0.94	−0.91	−0.91

where

$$P_{n+\frac{1}{2}}(k\rho) = 1 + \sum_{\substack{q=2 \\ q \text{ even}}}^{q=n} (-1)^{q/2} \cdot \frac{n(n+q)\prod_{i=1}^{i=q/2}[n^2-(q-i)^2]}{2^q q!(k\rho)^q} \tag{48a}$$

$$Q_{n+\frac{1}{2}}(k\rho) = \sum_{\substack{q=1 \\ q \text{ odd}}}^{q=n} (-1)^{(q-1)/2} \cdot \frac{n(n+q)\prod_{i=1}^{i=(q+1)/2}[n^2-(q-i)^2]}{2^q q!(k\rho)^q} \cdot \tag{48b}$$

From these two expressions, the ratio of the terms T_q in the series is found to be

$$\frac{T_q}{T_{q-2}} = \frac{n^4\left[1-\left(\frac{q-1}{n}\right)^2\right]\left[1-\left(\frac{q-2}{n}\right)^2\right]}{2q(q-1)(k\rho)^2} \cdot \frac{n+q}{n+q-2} \cdot \tag{49}$$

The terms of the series are thus monotonically decreasing and alternating. Convergence is rapid for $k\rho > n^2$. Combining (47) and (48) and using only the first terms of the series yields

$$\delta_n(k\rho) \approx \tan^{-1}\left[\frac{\frac{-n(n+1)}{2k\rho}}{1-\frac{n(n^2-1)(n+2)}{8(k\rho)^2}}\right], \text{ radians} \quad k\rho \geq n^2 \tag{50}$$

where

$\delta_n(k\rho)$ = deviation from spherical wave.

It is convenient to define a far-field parameter τ, where

$$\tau = \frac{k\rho}{n^2} \cdot \tag{51}$$

Table I gives the phase error δ_n versus τ for both the approximate method (50) and by exact calculation.

APPENDIX B
ELIMINATION OF FEED SYSTEM BACKLOBE

Using the asymptotic relationship for small ψ,[19]

$$P_n^1(\cos\psi) \approx \frac{n(n+1)}{2}\sin\psi, \quad (1-\cos\psi) \ll 1 \tag{52}$$

and the symmetry relationship

$$P_n^1[\cos(\pi-\psi)] = (-1)^{n-1}P_n'(\cos\psi) \tag{53}$$

one obtains

$$\lim_{\psi\to\pi}\frac{P_n^1(\cos\psi)}{\sin\psi} = \frac{(-1)^{n-1}n(n+1)}{2} \tag{54a}$$

$$\lim_{\psi\to\pi}\frac{dP_n^2(\cos)}{d\psi} = \frac{-(-1)^{n-1}n(n+1)}{2} \cdot \tag{54b}$$

From (23) and (54), then,

$$f_n(\psi=\pi) = 0. \tag{55}$$

ACKNOWLEDGMENT

The author is indebted to A. Ludwig of the Jet Propulsion Laboratory for several interesting discussions on spherical waves and for stimulating the author's interest in performing the attendant computer programming.

REFERENCES

[1] P. W. Hannan, "Microwave antennas derived from the Cassegrain telescope," *IRE Trans. Antennas and Propagation*, vol. AP-9, pp. 140–153, March 1961.

[2] P. A. Jensen, "Designing Cassegrain antennas," *Microwaves*, vol. 1, December 1962.

[3] W. D. White *et al.*, "Scanning characteristics of two-reflector antenna systems," *1962 Internat'l Conv. Rec.*, pt. 1, p. 44–70.

[4] P. D. Potter, "Aperture illumination and gain of a Cassegrainian system," *IEEE Trans. Antennas and Propagation (Communications)*, vol. AP-11, pp. 373–375, May 1963.

[5] P. Foldes, "The capabilities of Cassegrain microwave optics systems for low noise antennas," in *Proc. 5th Agard Avionics Panel Conf.* (Oslo, Norway), vol. 4. New York: Pergamon, 1962, pp. 319–352.

[6] W. V. T. Rusch, "Scattering from a hyperboloidal reflector in a

Cassegrainian feed system," *IEEE Trans. Antennas and Propagation*, vol. AP-11, pp. 414–421, July 1963.

[7] ——, "A comparison of diffraction in Cassegrainian and Gregorian radio telescopes," *Proc. IEEE (Correspondence)*, vol. 51, pp. 630–631, April 1963.

[8] ——, "Phase error and associated cross-polarization effects in Cassegrainian-fed microwave antennas," *IEEE Trans. Antennas and Propagation*, vol. AP-14, pp. 266–275, May 1966.

[9] P. Foldes and S. G. Kamlos, "Theoretical and experimental study of wideband paraboloid antenna with central reflector feed," *RCA Rev.*, vol. 21, pp. 94–116, March 1960.

[10] P. D. Potter, "Unique feed system improves space antennas," *Electronics*, vol. 35, pp. 36–40, June 22, 1962.

[11] ——, "The design of a very high power, very low noise Cassegrain feed system for a planetrary radar," in *Radar Techniques for Detection Tracking and Navigation, AGARDograph 100*. New York: Gordon and Breach Science Publishers.

[12] K. A. Green, "Modified Cassegrain antenna for arbitrary aperture illumination," *IEEE Trans. Antennas and Propagation (Communications)*, vol. AP-11, pp. 589–590, September 1963.

[13] V. Galindo, "Design of dual reflector antennas with arbitrary phase and amplitude distributions," *IEEE Trans. Antennas and Propagation*, vol. AP-12, pp. 403–408, July 1964.

[14] W. F. Williams, "High efficiency antenna reflector," *Microwave J.*, vol. 8, pp. 79–82, July 1965.

[15] S. P. Morgan, "Some examples of generalized Cassegrainian and Gregorian antennas," *IEEE Trans. Antennas and Propagation*, vol. AP-12, pp. 685–691, November 1964.

[16] A. C. Ludwig, "Radiation pattern synthesis for circular aperture horn antennas," *IEEE Trans. Antennas and Propagation*, vol. AP-14, pp. 434–440, July 1966.

[17] J. A. Stratton, *Electromagnetic Theory*. New York: McGraw-Hill, 1941, ch. 7.

[18] C. J. Bouwkamp and H. B. G. Casimir, "On multipole expansions in the theory of electromagnetic radiation," *Physica*, vol. 20, pp. 539–554, 1954.

[19] E. Jahnke and F. Ende, *Tables of Functions*. New York: Dover, 1945.

[20] National Bureau of Standards, *Tables of Spherical Bessel Functions*, vols. 1 and 2. New York: Columbia University Press, 1947.

[21] S. L. Belousov, "Tables of normalized associated Legendre polynomials," in *Mathematical Tables Series*, vol. 18. New York: Macmillan, 1962.

[22] R. O. Gumprecht *et al.*, "Tables of the functions of first and second partial derivatives of Legendre polynomials," Engineering Research Institute, University of Michigan, Ann Arbor, 1951.

[23] T. T. Taylor, "A discussion of the maximum directivity of an antenna," *Proc. IRE (Correspondence)*, vol. 36, p. 1135, September 1948.

[24] R. E. Collin and S. Rothschild, "Evaluation of antenna Q," *IEEE Trans. Antennas and Propagation*, vol. AP-12, pp. 23–27, January 1964.

[25] R. Joerg Irmer, "Spherical antennas with high gain," *IEEE Trans. Antennas and Propagation (Communications)*, vol. AP-13, pp. 827–828, September 1965.

[26] L. J. Chu, "Physical limitations of omni-directional antennas," *J. Appl. Phys.*, vol. 19, pp. 1163–1175, December 1948.

[27] Hughes Aircraft Company, Fullerton, Calif., "Final report for low noise, high efficiency Cassegrain antenna studies," Contract NAS5-3282 (prepared for Goddard Space Flight Center, December 1963).

[28] A. C. Ludwig, Ed., "Computer programs for antenna feed system design and analysis," Jet Propulsion Lab., California Institute of Technology, Pasadena, Calif. Tech. Rept. 32-979 (to be published).

[29] S. Silver, Ed., "Microwave antenna theory and design," in *M.I.T. Radiation Laboratory Series*. New York: McGraw-Hill, 1949, p. 439.

A Technique for the Synthesis of Shaped-Beam Radiation Patterns with Approximately Equal-Percentage Ripple

R. F. HYNEMAN, MEMBER, IEEE, AND R. M. JOHNSON, SENIOR MEMBER, IEEE

Abstract—**A new pattern synthesis technique which leads to shaped-beam patterns of approximately equal percentage or dB ripple is discussed. The method is based on the controlled location of the zeros of the pattern function in the complex pattern plane with the relative displacement of these zeros from the real sin θ axis determining the magnitude of ripple obtained with the synthesized pattern. In applying the technique, the locations are approximately constrained by starting with a fan or sector pattern having known zero locations. The sector pattern is then warped or perturbed to the pattern of desired shape by deterministic perturbations of the zeros. It is found that the design ripple of the sector pattern is approximately maintained during this process. A trade-off exists between ripple magnitude and maximum normalized slope of the approximating pattern function. Independent control of ripple level within the shaped-beam region and of sidelobe level without is achieved. Several examples of shaped-beam patterns (including $\csc^2 \theta$ patterns) are presented and discussed.**

Manuscript received February 3, 1967; revised February 23, 1967, and June 13, 1967.

R. F. Hyneman is with Ground Systems Group, Hughes Aircraft Company, Fullerton, Calif.

R. M. Johnson was with Ground Systems Group, Hughes Aircraft Company, Fullerton, Calif. He is now with Cryodry Corporation, San Ramon, Calif.

I. Introduction

THE general problem of synthesis of a line source to approximate a given radiation pattern has been extensively treated. Often used methods include those of Dunbar[1] and the simplified form of the Woodward technique.[2] While easily applied, neither method provides a particularly optimum reproduction of the desired pattern function.

A classical method involves truncation of the inverse Fourier transform[3] which leads to patterns showing a